Wave power absorption with wave energy converters

KARA, Fuat

Chapter

WAVE POWER ABSORPTION WITH WAVE ENERGY CONVETERS

F. Kara*, PhD

Department of Engineering and Mathematics, Sheffield Hallam University, Sheffield, UK

ABSTRACT

Wave power absorption with Wave Energy Converters (WECs) arrays and isolated WEC is predicted with an in-house transient wave-multibody numerical tool of ITU-WAVE which uses time marching scheme to solve a Boundary Integral Equation (BIE) for the analyses of hydrodynamic radiation and exciting forces. The hydrodynamics part of the solution is solved as impulsive velocity problem. Mean interaction factor, which can have constructive or destructive effect and determines the performances of WECs, is approximated with different configurations. A discrete control of latching is used to increase the bandwidth of the efficiency of WECs. When latching control applied to WEC in the case of off-resonance condition it increases the amplitude of the motion as well as absorbed power. The effects of the separation distances between array system and heading angles on energy absorption in both sway and heave modes are studied with numerical simulations which show sway mode has wider bandwidth than heave mode. The wave interactions are stronger when the array systems are closer proximity, and these wave interactions reduce significantly and shifted to larger times when the separation distances increase. The perfect reflection of incident waves from a vertical wall is considered with method of images. The vertical wall effect plays significant role over hydrodynamic parameters as the radiation and exciting forces show quite different behaviour in the case of WECs with and without vertical wall in an array system. The numerical results show that the performance and wave power absorption with WECs arrays in front of vertical wall are much greater compared to WECs arrays without vertical wall effect. The satisfactory agreements are obtained when the present ITU-WAVE numerical results for different hydrodynamic parameters are compared with analytical and other published numerical results.

Keywords: wave power absorption, mean interaction factor, multibody interaction, method of images, transient wave Green function, boundary integral equation

* Corresponding Author's Email: fuat.kara@shu.ac.uk

INTRODUCTION

The current development pace of wave energy converters indicates the possibility of the deployment of these converters as arrays at commercial scale. The accurate predictions of wave loads, motion characteristics, and power requirements are of critically important for the design of these devices which are in sufficiently closer proximity to experience significant hydrodynamic interactions. The oscillation of each body radiates waves assuming that other bodies are not present. Some of these radiated waves that can be considered as incident waves interact with the bodies of the array causing diffraction phenomena while others radiate to infinity. The fluid response between arrays can affect overall power generation and could increase or decrease power generation compared to an isolated device. The power generation due to hydrodynamic interaction depends on separation distance, geometrical layout, direction of the incident wave, geometry in the array, incident wavelength, mooring configurations, control strategies.

ANALYTICAL FRAMEWORK

Literature Review

Wave energy from ocean waves can be absorbed with or without a coastal structures effect (e.g., a vertical wall) using isolated, linear, square, or rectangular WECs arrays. The efficiency of these options depends on the geometries of WECs and WECs array configurations, control strategies to maximise the absorb wave power (Kara, 2010), Power-Take-Off (PTO) systems, incoming wave heading angles, single mode of motion (e.g., heave or pitch) or multimode (e.g., heave and pitch). In addition to these parameters, in the case of WECs arrays in front of a vertical wall, the efficiency also depends on the separation distance between WECs (Kara, 2016a) as well as a vertical wall and WECs. Although the installations, operations, and maintenances of WECs arrays at the offshore environment increase the overall cost significantly, the overall cost can be reduced by integrating WECs arrays with other coastal structures or placing them in front of them. As expected, the significant amount of wave power can be absorbed with WECs arrays compared to isolated WEC. This is mainly due to the hydrodynamic interactions between a vertical wall and WECs arrays as well as nearly trapped waves in the gap of array configurations (Mustapa et.al., 2017; Zhao et.al., 2019a).

The high energy costs can also be reduced by optimising the geometry of WECs (to increase hydrodynamic performances), control strategies (to improve efficiencies), and mechanical components (to avoid energy loses). In addition, using already available grid systems would result in to avoid additional cost and environmental impact effects. When

the performance of WECs arrays in front of a vertical wall is compared with those of integration of WECs arrays with other maritime structures, it is found out that previous one shows the superiority although the deployments of mooring systems, installations, and maintenances are more challenging for WECs placed in front of a vertical wall (Mustapa et.al., 2017). This is mainly due to the improved efficiency of WECs arrays resulting from the optimised hydrodynamic interactions with the reflected waves from a vertical wall and WECs in an array system.

The behaviour and performance of WECs in front of a vertical wall are studied both experimentally and numerically to define the effect of hydrodynamic interactions between a vertical wall and WECs arrays. The separation distances between a vertical wall and WECs as well as between WECs arrays play significant role on the maximum wave power absorption and performance of the array systems due to vertical wall effects (Schay et.al., 2013). The wave interaction and nearly trapped waves in the gap of WECs as well as a vertical wall and WECs can be used to increase the competitiveness and enhance the efficiency of array system. The performances of WEC arrays are studied with options of integrating or placing them in front of other maritime structures using different configurations including stationary and floating systems (e.g., Oscillating Water Column, Overtopping, oscillating buoys) (Ning et.al., 2016; Contestabile et.al., 2016; He et.al., 2013).

Impulse Response Functions (IRFs) of WECs arrays in front of a vertical wall, which is considered as the symmetry lines, can be predicted with method of images to approximate the flow behaviour around WECs arrays. The isolated WEC or WECs in an array system and their images with this method are used for the prediction of the frequency dependent radiation added-mass and damping coefficients as well as exciting forces in a channel or in front of vertical wall (Newman, 2016; Zhao et.al., 2019b). Method of images considers the vertical wall as infinite wall (Konispoliatis et.al., 2020) assuming infinite length and perfect reflection of incident waves. Alternatively, the vertical wall can be also considered as a finite wall (Loukogeorgaki et.al., 2020) considering the effect of finite length of the vertical wall on the hydrodynamic performances of WECs in an array system.

Analytical and numerical methods in two and three dimensions are used for the prediction of the wave power absorption in front of a vertical wall which is the function of exciting and radiation forces. The frequency domain methods in two (McIver and Porter, 2016) or three dimensions (Zheng and Zhang, 2016; Schay et.al., 2013) as well as time domain methods with three-dimensional wave Green function can be used to predict for wave power absorption in front of a vertical wall. The strips in strip theory are used in two-dimensional methods in which the interaction effects between the strips are not considered. This limitation of two-dimensional methods can be removed using three dimensional methods as the interactions between discretised panels are taken automatically into account. As two and three-dimensional frequency domain methods are inherently linear,

nonlinear effect can only be considered with two- or three-dimensional time domain methods which are used in the present study.

There are three commonly used three-dimensional methods in both frequency and time domain to predict the hydrodynamic exciting and radiation forces of WECs in front of a vertical wall. These three-dimensional methods take the hydrodynamic interactions between WECs and a vertical wall as well as between WECs into account. Rankine panel (Nakos et.al., 1993; Kring and Sclavounos, 1995) and wave Green function methods in both frequency and time domains (Chang, 1977; Kara, 2020, 2016a, 2016b) are the most used Boundary Integral Equations Methods (BIEM) which are the numerical methods used to predict the hydrodynamic parameters of floating systems. As wave Green function satisfies the condition at infinity and free-surface boundary conditions automatically, hydrodynamic parameters are predicted by discretising the body surface only to satisfy the body boundary condition. However, in the case of Rankine panel methods, body boundary condition, condition at infinity and free-surface boundary conditions are satisfied numerically by discretising both some part of free surface and body surface which increase the computational time considerably. The third types of the methods are the analytical methods at which WEC geometries (e.g., sphere, vertical cylinder) are defined analytically. The analytical methods include direct matrix method (Kagemoto and Yue, 1986), plane wave analysis (Ohkusu, 1972) and point absorber (Budal, 1977). The direct matrix method is extensively used in academia and industry due to its accurate predictions of the hydrodynamic performances floating bodies in an array system.

The wave energy absorption from ocean waves with WEC arrays in front of a vertical wall did not have much attention in the open literature compared to the exploitation of WECs without vertical wall effect. The efficiency of WECs arrays can be increased using a vertical wall which magnifies the absorbed wave power. In the context of hydrodynamic performance of WECs in front of a vertical wall, most of the papers in the literature is focused on the exciting forces due to incident and diffracted waves whilst the hydrodynamic radiation forces due to oscillations of WECs in an array system did not get much attention. The shortcoming of the existence literature in these fields will be filled with the present work. In addition, to the best of the authors' knowledge, the free-surface transient wave Green function is not used before for the prediction of the hydrodynamic radiation and exciting force parameters of WECs arrays in front of a vertical wall. This is an additional novel contribution to the knowledge in this field by the present study.

Method of images assuming infinite vertical wall length is used in the present paper to predict the time dependent diagonal and interaction IRFs of exciting forces, which are the superposition of diffraction and Froude-Krylow forces, and radiation forces for 1x5, 2x5, 3x5, 4x5 and 5x5 sphere WECs arrays in front of a vertical wall at sway and heave modes. Fourier transform of IRFs is then used to obtain the frequency dependent exciting force amplitude as well as radiation added-mass and damping coefficients. These frequency dependent hydrodynamic parameters are then compared with other published numerical

and analytical results for the validation of the present three-dimensional ITU-WAVE numerical results. The absorbed wave power, which are the functions of the hydrodynamic exciting and radiation forces, is directly predicted in time domain taking the average of instantaneous wave power signals. The contribution of transient effects on numerical results for wave power prediction is avoided by using only last half of the instantaneous wave power signals.

METHOD

Equation of motion of WECs in an array system

The right-handed body-fixed Cartesian coordinate system $\vec{x} = (x, y, z)$ for the solution of initial value problem is used to determine the fluid flow around WECs arrays in front of a vertical wall as presented in Figure 1. The coordinate system is placed on the free-surface and coincides with z=0 or xy-plane whilst the origin of the coordinate system is on the middle of the vertical wall. The positive z- and x-directions are towards upward and forward respectively. WECs arrays in front of a vertical wall oscillates at their mean position due to impulsively exited incident waves at the origin of the body fixed coordinate system. The boundaries of initial-value problem are presented with surface at infinity S_∞, free surface $S_f(t)$, surface at interaction between body and free-surface $\Gamma(t)$, body surface $S_b(t)$, and surface of a vertical wall $S_{wl}(t)$ in Figure 1 (Kara, 2020).

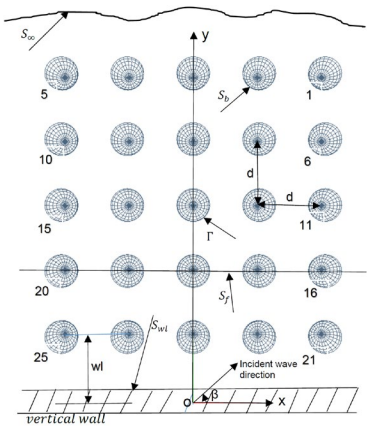

Figure 1. Coordinate system and surfaces of 5x5 WECs arrays of sphere in front of a vertical wall in xy-plane.

where the position of WECs in front of a vertical wall is given with numbers (1, 2, 3,…,25). The incident wave heading angles are presented with β and $\beta = 90°$ is for beam seas whilst $\beta = 180°$ is for head seas. d being separation distance between WECs and wl being separation distance between last row of WECs and the vertical wall.

The hydrodynamic performances of WECs arrays in time domain are solved assuming that fluid is inviscid and incompressible, and its flow is irrotational such that there are no lifting effects and fluid separation. These assumptions on fluid and its flow result in using the potential theory and implicitly also mean that the time dependent flow velocity $\vec{V}(\vec{x},t)$ can be represented as the gradient of the potential $\vec{V}(\vec{x},t) = \nabla\Phi(\vec{x},t)$. The use of potential theory also means that Laplace equation $\nabla^2\Phi(\vec{x},t) = 0$ dictates the solutions of the time dependent potentials $\Phi(\vec{x},t)$.

The time dependent equation of motion of WECs arrays in front of a vertical wall in Eq. (1) is the functions of acceleration relevant to inertia terms, hydrostatic restoring forces, and time dependent hydrodynamic restoring forces and exciting force parameters (Cummins 1962). The effects of the incident waves result in the pressure changes around WECs arrays which cause the oscillations of WECs. The oscillating WECs in an array system generates the radiated waves on the free surface which are presented by the convolution integral on the left-hand side of Eq. (1) whilst the effects of incident and diffracted waves are presented with convolution integral on the right-hand side of Eq. (1).

$$\sum_{k=1}^{6}\left(M_{kk_i}+a_{kk_i}\right)\ddot{x}_{k_i}(t)+\left(b_{kk_i}+B_{PTO-kk_i}\right)\dot{x}_{k_i}(t)+\left(C_{kk_i}+c_{kk_i}+C_{PTO-kk_i}\right)x_{k_i}(t) + \int_0^t d\tau K_{kk_i}(t-\tau)\dot{x}_{k_i}(\tau)=\int_{-\infty}^{\infty}d\tau K_{kD_i}(t-\tau)\zeta(\tau) \quad (1)$$

where upper boundary of sum $k = 1, 2, 3, \ldots, 6$ represents the mode of motions of surge, sway, heave, roll, pitch, and yaw respectively whilst index $i = 1, 2, 3, \ldots, N$ is for number of WECs in an array system. $x_k(t) = (1, 2, 3, \ldots, N)^T$, $\dot{x}_k(t)$ and $\ddot{x}_k(t)$, where dots represent time derivatives, is for displacements, velocities, and accelerations respectively. M_{kk} is the inertia mass matrix whilst C_{kk} is the hydrostatic restoring coefficients in Eq. (2). m and C are the inertia mass and restoring coefficient of an isolated WEC respectively. As the same radius R is used for all spheres in WECs arrays, the restoring force and inertia mass of each WEC are the same $C_1 = C_2 = \cdots = C_N = C$ and $m_1 = m_2 = \cdots = m_N = m$ respectively.

$$M_{kk} = \begin{pmatrix} m_1 & \cdots & 0 \\ \vdots & \ddots & \vdots \\ 0 & \cdots & m_N \end{pmatrix},\ C_{kk} = \begin{pmatrix} C_1 & \cdots & 0 \\ \vdots & \ddots & \vdots \\ 0 & \cdots & C_N \end{pmatrix} \quad (2)$$

The time and frequency independent restoring coefficient c_{kk}, damping coefficient b_{kk} and infinite added mass a_{kk} coefficients in Eq. (3) depend on geometry and are relevant to displacement, velocity, and acceleration respectively. The interaction terms are represented with off-diagonal terms whilst the diagonal terms represent the contribution of each WEC

in an array system. IRF $K_{kk}(t)$, which is the function of the time and geometry, represent the force on k-th body due to the impulsive velocity of k-th body. The oscillations of WECs in an array system cause the disturbance of free surface which is known as the memory effect of the fluid responses. The convolution integral on the left-hand side of Eq. (1) are used to represent the memory effect and the effect of the wave damping (Ogilvie 1964).

$$K_{kk}(t) = \begin{pmatrix} K_{11} & \cdots & K_{1N} \\ \vdots & \ddots & \vdots \\ K_{N1} & \cdots & K_{NN} \end{pmatrix}, a_{kk} = \begin{pmatrix} a_{11} & \cdots & a_{1N} \\ \vdots & \ddots & \vdots \\ a_{N1} & \cdots & a_{NN} \end{pmatrix}, b_{kk} = \begin{pmatrix} b_{11} & \cdots & b_{1N} \\ \vdots & \ddots & \vdots \\ b_{N1} & \cdots & b_{NN} \end{pmatrix},$$
$$c_{kk} = \begin{pmatrix} c_{11} & \cdots & c_{1N} \\ \vdots & \ddots & \vdots \\ c_{N1} & \cdots & c_{NN} \end{pmatrix} \quad (3)$$

The origin of the body-fixed coordinate system in Figure 1 is used to predict the time dependent exciting force IRFs $K_{kE}(t) = (K_{1E}, K_{2E}, K_{3E}, \dots, K_{NE})^T$ on the k-th body due to impulsive incident wave elevation $\zeta(t)$, which is a uni-directional incoming wave system with arbitrary heading angles, as presented in Eq. (4). The superposition of diffraction and Froude-Krylov IRFs results in the exciting forces and moments $K_{kE}(t)$ in time on the right-hand side of Eq. (1) (King, 1987).

$$F_{kE}(t) = \int_{-\infty}^{\infty} d\tau K_{kE_i}(t-\tau)\zeta(\tau) \qquad (4)$$

The elements of PTO in Eq. (5) are the time independent and frequency dependent wave damping coefficient B_{PTO-kk} matrix and C_{PTO-kk} which is the time and frequency independent restoring coefficient matrix. It is theoretically known that the maximum wave power is absorbed at the resonant frequency (Budal and Falnes, 1976). It is the reason that the diagonal elements of PTO matrix B_{PTO-kk} in Eq. (5) are selected as the wave damping at the resonant frequency at which the natural frequency of isolated WEC and incident wave excitation frequency are equal. For the simplicity purpose, the off-diagonal terms of PTO matrix, which represent the wave damping due to cross-interaction between WECs in an array system, are considered zero. The elements of C_{PTO-kk} are considered zero for heave mode while for sway mode, the diagonal elements of C_{PTO-kk} are taken the same as hydrostatic restoring coefficient of heave mode to have the same natural frequency and displacement in both heave and sway modes. In this case, it would be possible to compare heave and sway motions and power variables directly to decide which modes of motion are more effective and efficient for power absorption.

$$B_{PTO-kk} = \begin{pmatrix} B_{iso}(\omega_n) & \cdots & 0 \\ \vdots & \ddots & \vdots \\ 0 & \cdots & B_{iso}(\omega_n) \end{pmatrix}, \; C_{PTO-kk} = \begin{pmatrix} C_1 & \cdots & 0 \\ \vdots & \ddots & \vdots \\ 0 & \cdots & C_N \end{pmatrix} \quad (5)$$

where the natural frequency of each isolated WEC is given with ω_n. The time marching scheme with fourth order Runge-Kutta method (Kara 2016b, 2015) can be used to solve the equation of motion Eq. (1) after determination of PTO damping B_{PTO-kk}, restoring C_{PTO-kk} matrices, and inertia mass matrix M_{kk}. The time and frequency independent added-mass at infinite wave frequency a_{kk}, wave damping b_{kk} and restoring c_{kk} coefficients are also input for Eq. (1). In addition, Eq. (1) at each time step requires the hydrodynamic restoring or wave damping which is represented with convolution integral on the left-hand side of Eq. (1) and is the function of the radiation IRFs and velocity of WECs. Furthermore, the exciting force at each time step is also required and represented with convolution integral on the right-hand side of Eq. (1).

Integral equation of WECs in an array system

The transient wave Green function is used to solve the initial value problem which can be modelled as a surface integral equation and requires the satisfaction of the initial condition, free surface boundary condition, body boundary condition and condition at infinity. The transient wave Green function satisfy the free-surface boundary condition and condition at infinity automatically which means only body boundary condition need to be satisfied numerically (Wehausen and Laitone, 1960). The transient integral equation of the source strength in time on WECs in an array system (Kara, 2020) is obtained by applying Green's theorem with the properties of the transient wave Green function and potential theory in Eq. (6).

$$\begin{cases} \sigma_1(\mathrm{P},\mathrm{t}) + \frac{1}{2\pi}\iint_{\mathrm{S}_1} \mathrm{dS_Q} \frac{\partial}{\partial \mathrm{n_P}} \mathrm{G}(\mathrm{P},\mathrm{Q},\mathrm{t}-\tau)|_{\mathrm{S}_1} \sigma_1(\mathrm{Q},\mathrm{t}) + \cdots + \frac{1}{2\pi}\iint_{\mathrm{S}_N} \mathrm{dS_Q} \frac{\partial}{\partial \mathrm{n_P}} \mathrm{G}(\mathrm{P},\mathrm{Q},\mathrm{t}-\tau)|_{\mathrm{S}_1} \sigma_N(\mathrm{Q},\mathrm{t}) = -2\frac{\partial}{\partial \mathrm{n_P}} \phi(\mathrm{P},\mathrm{t})|_{\mathrm{S}_1} \\ \vdots \\ \sigma_N(\mathrm{P},\mathrm{t}) + \frac{1}{2\pi}\iint_{\mathrm{S}_1} \mathrm{dS_Q} \frac{\partial}{\partial \mathrm{n_P}} \mathrm{G}(\mathrm{P},\mathrm{Q},\mathrm{t}-\tau)|_{\mathrm{S}_N} \sigma_1(\mathrm{Q},\mathrm{t}) + \cdots + \frac{1}{2\pi}\iint_{\mathrm{S}_N} \mathrm{dS_Q} \frac{\partial}{\partial \mathrm{n_P}} \mathrm{G}(\mathrm{P},\mathrm{Q},\mathrm{t}-\tau)|_{\mathrm{S}_N} \sigma_N(\mathrm{Q},\mathrm{t}) = -2\frac{\partial}{\partial \mathrm{n_P}} \phi(\mathrm{P},\mathrm{t})|_{\mathrm{S}_N} \end{cases} \quad (6)$$

and the time dependent potential on each WEC in an array system

$$\begin{cases} \phi_1(\mathrm{P},\mathrm{t}) = -\frac{1}{4\pi}\iint_{\mathrm{S}_1} \mathrm{dS_Q} \mathrm{G}(\mathrm{P},\mathrm{Q},\mathrm{t}-\tau)|_{\mathrm{S}_1} \sigma_1(\mathrm{Q},\mathrm{t}) - \cdots - \frac{1}{4\pi}\iint_{\mathrm{S}_N} \mathrm{dS_Q} \mathrm{G}(\mathrm{P},\mathrm{Q},\mathrm{t}-\tau)|_{\mathrm{S}_1} \sigma_N(\mathrm{Q},\mathrm{t}) \\ \vdots \\ \phi_N(\mathrm{P},\mathrm{t}) = -\frac{1}{4\pi_1}\iint_{\mathrm{S}_1} \mathrm{dS_Q} \mathrm{G}(\mathrm{P},\mathrm{Q},\mathrm{t}-\tau)|_{\mathrm{S}_N} \sigma_1(\mathrm{Q},\mathrm{t}) - \cdots - \frac{1}{4\pi}\iint_{\mathrm{S}_N} \mathrm{dS_Q} \mathrm{G}(\mathrm{P},\mathrm{Q},\mathrm{t}-\tau)|_{\mathrm{S}_N} \sigma_N(\mathrm{Q},\mathrm{t}) \end{cases} \quad (7)$$

where the transient Green function, which has time dependent and time independent parts, is given by $\mathrm{G}(\mathrm{P},\mathrm{Q},\mathrm{t}-\tau) = \left(\frac{1}{\mathrm{r}} - \frac{1}{\mathrm{r}'}\right)\delta(\mathrm{t}-\tau) + \mathrm{H}(\mathrm{t}-\tau)\widetilde{\mathrm{G}}(\mathrm{P},\mathrm{Q},\mathrm{t}-\tau)$ where the time

independent part is known as Rankine parts and are presented with $\left(\frac{1}{r}-\frac{1}{r'}\right)$ whilst the time dependent part is known as transient or memory part and is given by $\widetilde{G}(P,Q,t-\tau)$ that present the free surface effect due to oscillation of WECs in an array system. The interactions of the discretised surface panels are given with $r=\sqrt{(x-\xi)^2+(y-\eta)^2+(z-\zeta)^2}$ which represents the distance between field points $P(x,y,z)$ and source or integration points $Q(\xi,\eta,\zeta)$ whilst the image part that is distance between field point and image integration point above free surface is presented with $r'=\sqrt{(x-\xi)^2+(y-\eta)^2+(z+\zeta)^2}$. Dirac delta function and Heaviside unit step function are presented with $\delta(t-\tau)$ and $H(t-\tau)$ respectively. WECs in an array system are discretised with quadrilateral panel and analytical integrations (Hess and Smith 1964) are used to predict the solution of Rankine part $\left(\frac{1}{r},\frac{1}{r'}\right)$. The mixed solution methods for the surface integration are used depending on the distance between field point $P(x,y,z)$ and integration points $Q(\xi,\eta,\zeta)$. The exact solution, a multi-pole extension and a monopole expansion are used for the small, intermediate, and large values of r (P,Q) respectively.

$\widetilde{G}(P,Q,t-\tau)=2\int_0^\infty dk\sqrt{kg}\sin(\sqrt{kg}(t-\tau))e^{k(z+\zeta)}J_0(kR)$ represents the transient or memory part where $J_0(kR)$ is the zero order Bessel function, k being wave number, $R=\sqrt{(x-\xi)^2+(y-\eta)^2}$ being the distance between field point $P(x,y,z)$ and integration point $Q(\xi,\eta,\zeta)$ on the free surface, and g being gravitational acceleration. In the case of transient part, $P(x(t),y(t),z(t))$ is the time dependent potential at time t which is due to an impulsive disturbance at time dependent integration point $Q(\xi(t),\eta(t),\zeta(t))$ and time τ. The solution of transient wave part $\widetilde{G}(P,Q,t-\tau)$ of Green function $G(P,Q,t-\tau)$ over quadrilateral panels are mapped into a unit square and then are integrated numerically with 2x2 two-dimensional Gaussian quadrature after the solution of the transient wave Green function analytically $\widetilde{G}(P,Q,t-\tau)$ (Liapis 1986, King 1987, Kara 2000). The prediction of memory part $\widetilde{G}(P,Q,t-\tau)$ is the computationally expensive so that it is important to use accurate and efficient methods. As only one kind of analytical method cannot be used for the solution due to convergence problems, five analytical methods depending on time and space parameters, which are function of relative position of field and integration points, are used to predict the time dependent wave Green function $\widetilde{G}(P,Q,t-\tau)$ part including asymptotic expansion of complex error function, Bessel function, Filon quadrature, an asymptotic expansion, and power series expansion.

The time dependent potentials $(\phi_1,\phi_2,\phi_3,\dots,\phi_N)$ in Eq. (7), N being the number of WECs in an array system, is predicted with time marching scheme after the solution of the time dependent integral equations for source strengths $(\sigma_1,\sigma_2,\sigma_3,\dots,\sigma_N)$ in Eq. (6). The time dependent fluid velocities are then calculated as the gradient of the potentials $(\nabla\phi_1,\nabla\phi_2,\nabla\phi_3,\dots,\nabla\phi_N)$. As the only difference for the solution of the integral equation of the radiation and diffraction problems is time dependent boundary conditions, which are the terms on the right-hand-side of Eq. (6), Eq. (6) can be used for the predictions of both radiation and diffraction time dependent source strengths $(\sigma_1,\sigma_2,\sigma_3,\dots,\sigma_N)$, which

describe the flow behaviour around WECs in an array system. As the condition at infinity and free-surface boundary condition are satisfied automatically by the transient wave Green Function part $\widetilde{\mathrm{G}}(\mathrm{P},\mathrm{Q},\mathrm{t}-\tau)$, only the body surfaces beneath free surface of WECs in an array system is discretised with quadrilateral elements over which the constant source strengths are used for the solution of the integral equation Eq. (6) in time. The discretisation of the surfaces of WECs in an array system implies that unknown finite number of the source strengths $(\sigma_1,\sigma_2,\sigma_3,\dots,\sigma_\mathrm{N})$ are replaced with continuous singularity distributions. The collocation points of each quadrilateral elements are used to satisfy the integral equation Eq. (6) which results in a system of algebraic equation for the prediction of the time dependent source strengths $(\sigma_1,\sigma_2,\sigma_3,\dots,\sigma_\mathrm{N})$ on each quadrilateral element.

Instantaneous and mean absorbed wave power

The instantaneous wave energy $P_{ins_{k_i}}(t)$ from ocean waves is converted to useful electrical energy at each mode of motion from each WEC in an array system with PTO system. The time dependent instantaneous absorbed wave power $P_{ins_{k_i}}(t)$ is presented in Eq. (8) and is the functions of exciting force, radiation force, and velocity of each WEC placed in front of a vertical wall.

$$P_{ins_{k_i}}(t) = [F_{exc_{k_i}}(t) + F_{rad_{k_i}}(t)] \cdot \dot{x}_{k_i}(t) \qquad (8)$$

where $F_{exc_{k_i}}(t)$ Eq. (9) being time dependent exciting force due to incident and diffracted waves and $F_{rad_{k_i}}(t)$ Eq. (10) being radiation force due to oscillation of each WEC in an array system whilst the velocities of each WEC in front of a vertical wall are presented with $\dot{x}_{k_i}(t)$ (Kara 2010, 2016a).

$$F_{exc_{k_i}}(t) = F_{k_i}(t) = \int_{-\infty}^{\infty} d\tau K_{kD_i}(t-\tau)\zeta(\tau) \quad (9)$$

$$\begin{aligned} F_{rad_{k_i}}(t) = F_{kk_i}(t) \\ &= -a_{kk_i}\ddot{x}_{k_i}(t) - b_{kk_i}\dot{x}_{k_i}(t) - c_{kk_i}x_{k_i}(t) \\ &\quad - \int_0^t d\tau K_{kk_i}(t-\tau)\dot{x}_{k_i}(\tau) \end{aligned} \qquad (10)$$

The product of time dependent exciting force $F_{exc_{k_i}}(t)$ Eq. (9) and WEC velocity $\dot{x}_{k_i}(t)$ results in the absorbed total exciting wave power $P_{exc_{k_i}}(t) = F_{exc_{k_i}}(t) \cdot \dot{x}_{k_i}(t)$ from incident wave at any heading angles. The product of time dependent velocity $\dot{x}_{k_i}(t)$ and radiation force $F_{rad_{k_i}}(t)$ Eq. (10) results in radiation wave power $P_{rad_{k_i}}(t) = F_{rad_{k_i}}(t) \cdot$

$\dot{x}_{k_i}(t)$ which is the power that is radiated back to sea. The absorbed mean wave power $\bar{P}_{ins_{k_i}}(t)$ with PTO system from ocean waves over a range of time T in Eq. (11) is averaged to predict the absorbed useful wave power.

$$\bar{P}_{ins_{k_i}}(t) = \frac{1}{T}\int_0^T dt \cdot [F_{exc_{k_i}}(t) + F_{rad_{k_i}}(t)] \cdot \dot{x}_{k_i}(t) \quad (11)$$

Eq. (11) is approximated directly with numerical integration

$$\bar{P}_{ins_{k_i}}(t_j) \cong \frac{1}{n_j}\sum_{j=1}^{n_j} [F_{exc_{k_i}}(t_j) + F_{rad_{k_i}}(t_j)] \cdot \dot{x}_{k_i}(t_j) \quad (11a)$$

where $j = 1, 2, 3, \ldots, t_N$, t_N being total number of time step, n_j is the number of samples ($T = n_j \Delta t$), Δt being time step size. The transient effects are avoided considering only the last half of the simulation to predict the time dependent parameters including the averaged (mean) absorbed wave power in Eq. (11a).

$$\bar{P}_{T_k}(t) = \sum_{i=1}^{N} \bar{P}_{ins_{k_i}}(t) \quad (12)$$

The time dependent absorbed total mean wave power $\bar{P}_{T_k}(t)$ in Eq. (12) at mode of motion of k is the superposition of the mean wave power that is absorbed with each $i-th$ WEC in an array system in front of a vertical wall with N numbers of WECs.

Mean interaction factor

The mean interaction factor $q_{mean,k}(\omega)$ at any incident wave frequency is used to measure the gain factor due to the interaction of WECs in an array system in front of a vertical wall and is the function of wave power absorbed by N interacting WECs and isolated WEC at any given heading angles. The constructive ($q_{mean,k}(\omega) > 1$) and destructive ($q_{mean,k}(\omega) < 1$) effects of mean interaction factor $q_{mean,k}(\omega)$ depend on the separation distance between WECs as well as a vertical wall and WECs, incident wave heading angles, geometry of WECs, and control strategies to improve the efficiency of WECs in an array system.

The frequency dependent mean interaction factor at any incident wave frequency in Eq. (13) is given as the ratio of the sum of mean absorbed wave power with N number of

WECs in an array system in front of a vertical wall to N times the mean absorbed wave power with an isolated WEC at the resonant frequency (Thomas & Evans 1981).

$$q_{mean,k}(\omega) = \frac{\bar{P}_{T_k}(\omega)}{N \times \bar{P}_{ins_{k_0}}(\omega_n)} \quad (13)$$

where N is the number of WECs in an array system. The sum of the mean absorbed wave power at any mode of motion k is given with $\bar{P}_{T_k}(\omega)$ at any given incident wave frequency ω whilst the mean absorbed wave power with an isolated WEC is given with $\bar{P}_{ins_{k_0}}(\omega_n)$ at the resonant frequency ω_n.

RESULTS AND DISCUSSION

The present numerical results of hydrodynamic parameters (e.g., exciting and radiation IRFs, exciting force amplitudes, added-mass and damping coefficients) and wave power absorptions from ocean waves with WECs in an array system with and without a vertical wall effect are predicted with in-house transient wave-multibody interaction computational code of ITU-WAVE (Kara, 2021a, 2021b, 2021c, 2020a, 2021b, 2017, 2016a, 2016b, 2016c, 2015, 2011, 2010, 2000).

Validation of ITU-WAVE numerical results with analytical and numerical results

The present ITU-WAVE numerical results of diagonal and interaction added-mass and damping coefficients, exciting force amplitudes, and mean interaction factors of absorbed wave power are validated against different configurations of WECs arrays including 1x5 and 2x2 arrays of truncated vertical cylinder in front of a vertical wall and 2x5 arrays of vertical cylinder with hemisphere bottom without vertical wall effect.

Truncated vertical cylinder of 1x5 arrays in front of a vertical wall – radiation forces

The method of images in the present ITU-WAVE is used to predict the hydrodynamic parameters of 1x5 linear arrays of truncated vertical cylinders. The analytical results of Konispoliatis et.al. (2020) is then used for the validation of ITU-WAVE numerical results. The convergence test is conducted in space and time which are converged with 256 panels for each WEC in space and 0.05 nondimensional time step size $\Delta t\sqrt{g/R}$ in time. When surge and sway mode nondimensional diagonal IRFs are compared in Figure 2(a), it can be observed that surge IRF decays faster at larger nondimensional time steps of 15 and 25. As the area under IRFs represents the energy to be captured (Kara, 2020, 2016a), this

implicitly means that sway mode stores more energy at larger times compared to surge mode. The nondimensional interaction IRFs in sway mode between WEC1 and WEC2 (K_{12}) as well as between WEC1 and WEC3 (K_{13}) are shown in Figure 2(b). The behaviour of diagonal IRF in Figure 2(a) and interaction IRFs in Figure 2(b) in sway mode are quite different. The interaction IRFs show greater oscillation amplitudes at larger times whilst diagonal IRF decays to zero just after nondimensional time step of 4. It can be also seen in Figure 2(b) that when the separation distances between WECs increase, the interaction strength or oscillation amplitude decreases which implicitly means that available wave energy from ocean waves to capture decreases. This can be clearly observed in Figure 2(b) between sway IRFs of K_{12} and K_{13}.

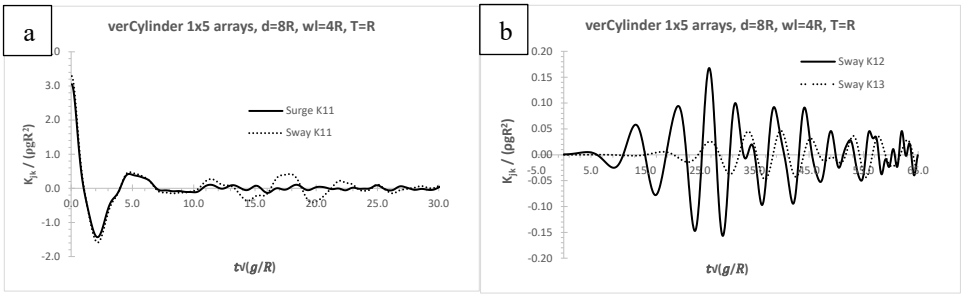

Figure 2. Linear 1x5 arrays of truncated vertical cylinder in front of a vertical wall with radius R, d=8R, wl=4R, draft T=R; (a) surge and sway diagonal IRFs of K_{11} for WEC1; (b) sway interaction IRFs of K_{12} and K_{13}.

Figure 3(a) and (b) show the dimensionless diagonal added-mass and damping coefficients in surge mode for 1x5 arrays of truncated vertical cylinder, respectively. The present ITU-WAVE numerical results are compared with analytical results of Konispoliatis et.al. (2020). The comparison of present numerical results with analytical results shows satisfactory agreements as can be seen in Figure 3(a) and (b). In the context of linear analysis, time and frequency domain results are dependent on each other through Fourier transform. The frequency dependent added-mass Figure 3(a) and damping Figure 3(b) coefficients are obtained by taking Fourier transform of time dependent diagonal surge IRFs K_{11} of Figure 2(a).

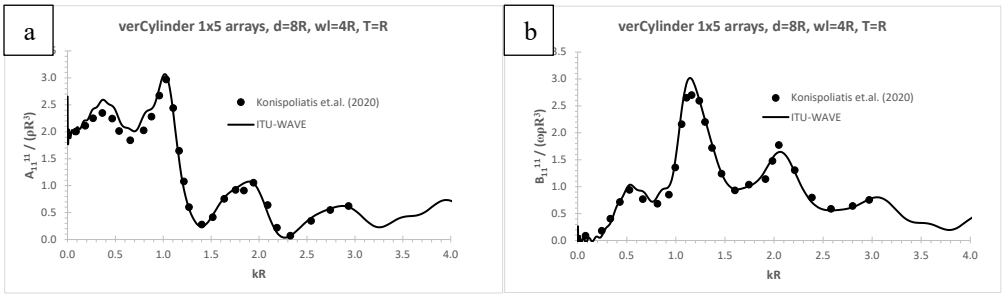

Figure 3. Surge dimensionless diagonal radiation force coefficients; (a) added-mass; (b) damping coefficients of WEC1.

Figure 4(a) and (b) show the dimensionless interaction added-mass and damping coefficients in sway mode between WEC1 and WEC2 for 1x5 arrays of truncated vertical cylinder. The present ITU-WAVE results are compared with analytical results (Konispoliatis et.al. 2020) which show satisfactory agreements.

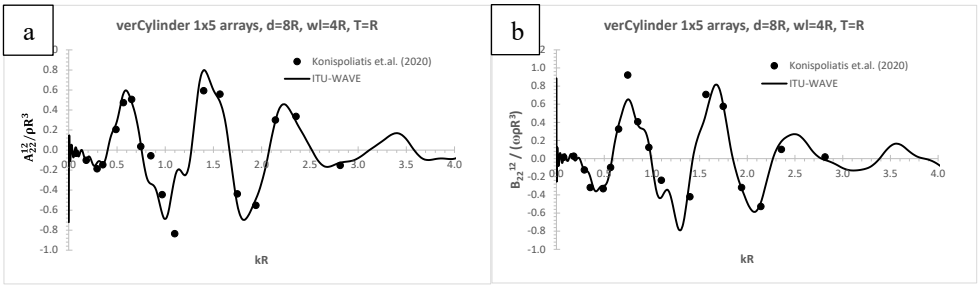

Figure 4. Sway dimensionless radiation interaction force coefficients between WEC1 and WEC2; (a) added-mass; (b) damping coefficients.

Truncated vertical cylinder of 2x2 arrays in front of a vertical wall – exciting forces

The nondimensional exciting IRFs in sway mode for 2x2 arrays of truncated vertical cylinder at incident wave angle of 270º are presented in Figure 5. The exciting IRFs for WEC1 and WEC2 as well as WEC3 and WEC4 are the same due to the symmetry of WECs with respect to the heading angle of 270º.

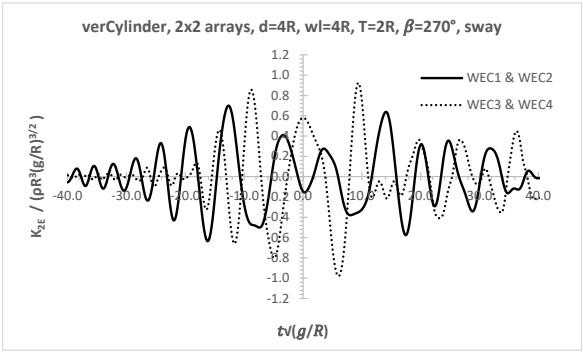

Figure 5. Sway nondimensional exciting force IRFs of square 2x2 arrays of truncated vertical cylinder in front of a vertical wall.

The dimensionless sway exciting force amplitudes of square 2x2 arrays of truncated vertical cylinders at the incident wave angle of 270º are compared with the numerical results of Chatjigeorgiou (2019) for WEC1 & WEC2 and WEC3 & WEC4 in Figure 6(a) and 6(b) respectively. The present frequency dependent sway exciting force amplitudes of ITU-WAVE numerical results and those of Chatjigeorgiou (2019) show satisfactory

agreements. The wave exciting force amplitudes for WEC1 and WEC2 as well as WEC3 and WEC4 are obtained via Fourier transform of exciting IRFs of Figure 5 in sway mode. As in sway exciting IRFs of Figure 5, the exciting force amplitude of WEC1 and WEC2 as well as WEC3 and WEC4 are the same due to the symmetry of WECs with respect to incident wave angle of 270°.

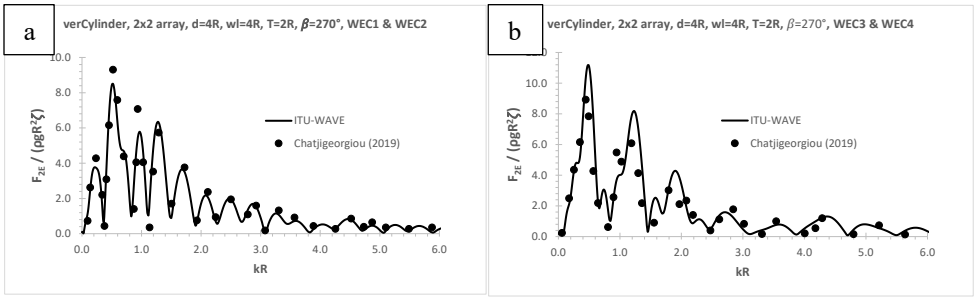

Figure 6. Sway nondimensional exciting force amplitudes; (a) WEC1 and WEC2; (b) WEC3 and WEC4.

Vertical cylinder with hemisphere bottom of 2x5 arrays – mean interaction factor

The heave exciting force IRFs and amplitudes of 2x5 arrays of vertical cylinder with hemisphere bottom are presented in Figure 7(a) and 7(b) respectively. It may be noticed in Figure 7(a) and 7(b) that heave exciting IRFs and force amplitudes of WEC1, WEC2, WEC3, WEC4, WEC5 and WEC6, WEC7, WEC8, WEC9, WEC10 are the same due to the symmetry of WECs with respect to incident wave angle of 90°.

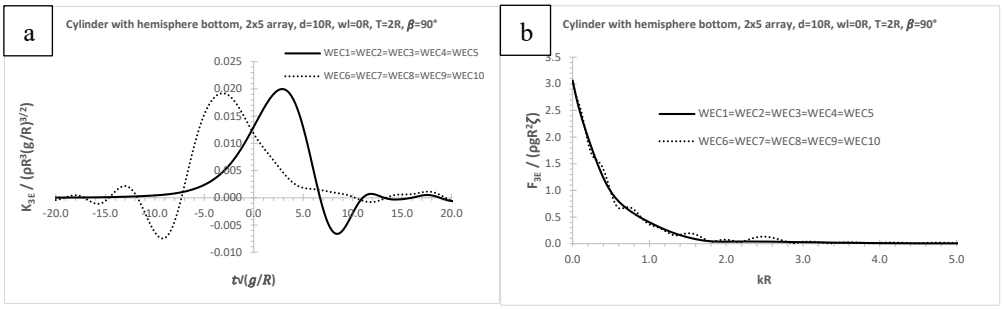

Figure 7. Heave dimensionless exciting force of rectangle 2x5 arrays of vertical cylinder with hemisphere bottom without wall effect; (a) IRFs; (b) exciting force amplitudes.

The dimensionless heave diagonal and interaction radiation IRFs are presented in Figure 8(a) and 8(b). When heave diagonal K_{11} IRF is compared with interaction K_{12}, K_{13}, K_{14} and K_{15} where K_{15} represents the interaction IRF between WEC1 and WEC5, it can be observed in Figure 8(a) that diagonal IRF is almost 8 times greater than interaction IRFs. When the separation distances between WECs increase in Figure 8(b), the amplitudes of interaction IRFs decrease. This implicitly means that hydrodynamic interactions between WECs are weaker. The interaction IRFs decay to zero after a few oscillations in the case

of closer proximity (e.g., K_{16}, K_{17}) in Figure 8(b) whilst, when the separation distance between WECs increases, it takes longer times for interaction IRFs to decay to zero and oscillations with greater amplitudes shift to longer times (e.g., K_{19}, K_{110}).

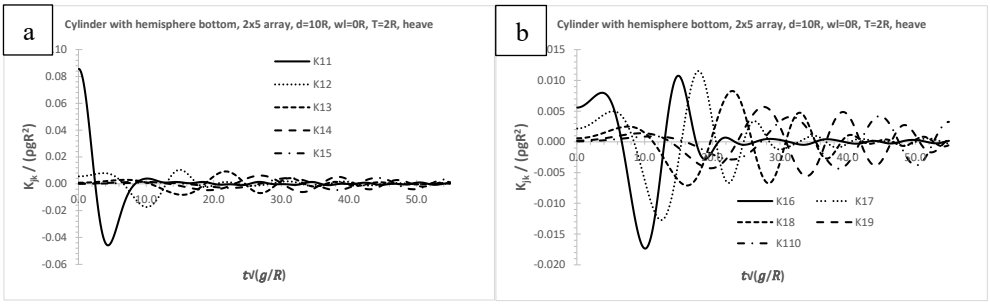

Figure 8. Heave dimensionless diagonal and interaction radiation force IRFs; (a) $K_{11} - K_{15}$; (b) $K_{16} - K_{110}$.

The dimensionless heave diagonal and interaction hydrodynamic coefficients are presented in Figure 9(a) and 9(b) for added-mass and in Figure 10(a) and 10(b) for damping coefficients. Figure 9(a) and 10(a) represent the diagonal and interaction added-mass and damping coefficients of 1st row of 2x5 arrays whilst 2nd row results are presented in Figure 9(b) and 10(b) respectively. When the separation distances increase between WECs, the amplitudes of interaction added-mass and damping coefficients decrease in Figure 9(b) and 10(b). It may be also noticed that when the separation distances increase between WECs, the interaction added-mass and damping coefficients require more oscillation to decay to zero.

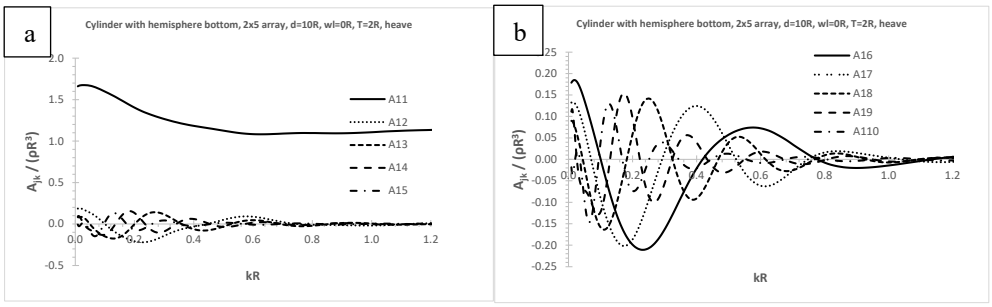

Figure 9. Heave dimensionless diagonal and interaction added-mass coefficients; (a) A_{11}- A_{15}; (b) A_{16}- A_{110}.

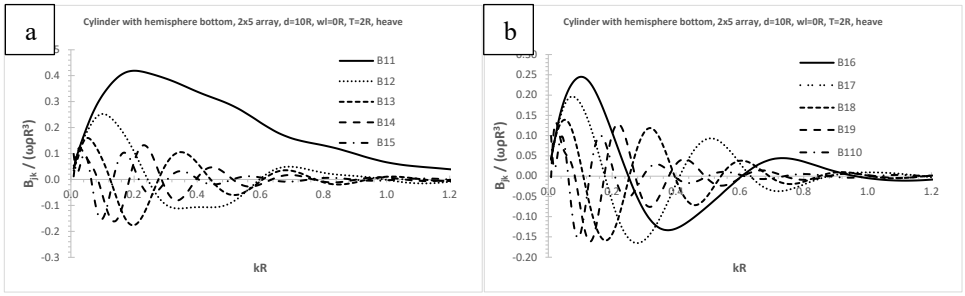

Figure 10. Heave dimensionless diagonal and interaction damping coefficients; (a) B_{11}- B_{15}; (b) B_{16}- B_{110}.

The predicted mean interaction factor of ITU-WAVE is compared with numerical result of McCallum et.al. (2014) in Figure 11. The present ITU-WAVE numerical result shows satisfactory agreement with that of McCallum et.al. (2014). In addition to mean interaction factor, which is the sum of mean interaction factor of 1st row (WEC1-WEC5) and 2nd (WEC6-WEC10) row of 2x5 arrays system, the mean interaction factors of 1st and 2nd rows are also presented in Figure 11. The mean interaction factor of 2nd row, which is in the wake of 1st row that meets with the incident wave first, is greater and has more constructive effect compared to 1st row. This is mainly due to the strong hydrodynamic interactions and nearly trapped waves in the gap of 1st and 2nd rows of WECs in an array system. The mean interaction factor has maximum constructive effect at dimensionless natural frequency of 0.5 whilst it has destructive effect at about dimensionless incident wave frequency of 0.6. The mean interaction factor oscillates about q_{mean} = 1.0 up to dimensionless incident wave frequency of 0.4 which means that the same amount of wave energy from ocean waves is absorbed with isolated WECs and rectangle 2x5 arrays whilst mean interaction factor has mainly constructive effects at dimensionless higher incident wave frequencies.

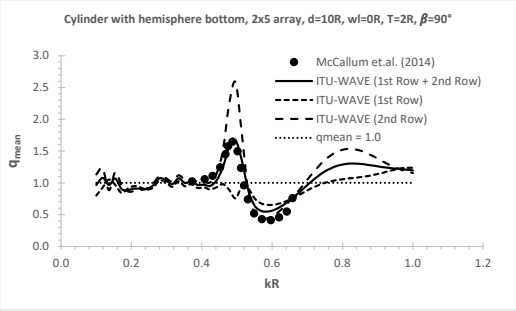

Figure 11. Mean interaction factor q_{mean} of rectangle 2x5 arrays of vertical cylinder with hemisphere bottom without a vertical wall effect.

Radiation and exciting force IRFs

The dimensionless exciting force IRFs of 1x5 arrays of sphere with radius R are presented in Figure 12. The IRFs for WEC1 and WEC5 as well as WEC2 and WEC4 are the same due to symmetry of WECs with respect to heading angle of 90° for both with and without vertical wall effects. When with and without vertical wall effects are compared, the bandwidth of the IRFs with vertical wall effects are greater than that of without vertical wall effect. As the area under IRFs represents the available energy to absorb with WECs, Figure 12 implicitly shows that more energy is available in the case of WECs arrays in front of a vertical wall due to wider bandwidths. The IRFs with vertical wall effects start to oscillate much earlier. This also implicitly means that WECs in an array system feel the effect of incident waves earlier in the case of WECs placed in front of a vertical wall.

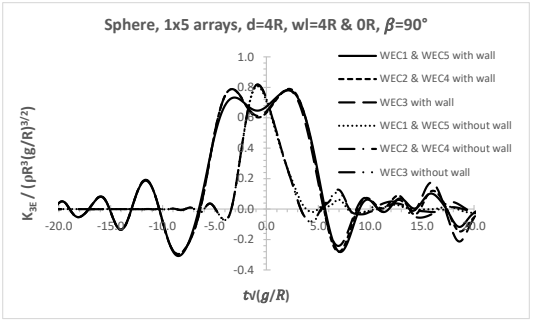

Figure 12. Heave dimensionless exciting force IRFs of 1x5 arrays of sphere with and without vertical wall effects.

The dimensionless heave exciting force IRFs at the middle of each row of 5x5 arrays of sphere without and with vertical wall effects are presented in Figure 13(a) and 13(b) respectively. Although the exciting force amplitudes of IRFs without and with vertical wall effects are approximately the same, the bandwidth of heave exciting force IRFs are greater in the case of WECs arrays in front of a vertical wall. This implicitly means that as mentioned before, more wave energy from ocean waves would be absorbed with WECs arrays placed in front of a vertical wall.

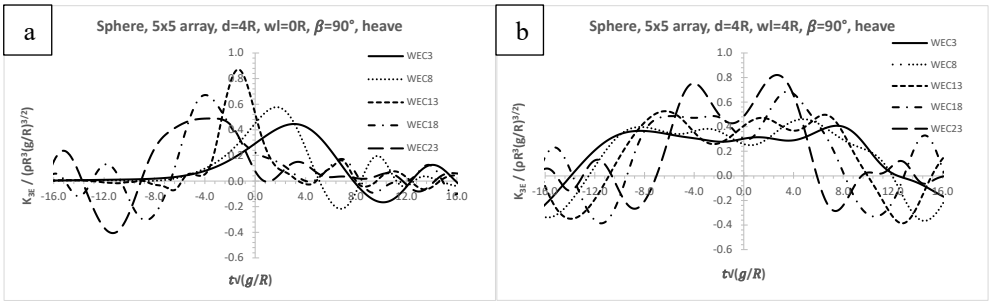

Figure 13. Heave dimensionless exciting force IRFs at the middle of each row of 5x5 arrays of sphere; (a) without vertical wall effect; (b) with vertical wall effect.

The dimensionless heave radiation interaction IRFs of 1x5 arrays of sphere without and with vertical wall effects are presented in Figure 14(a) and 14(b) respectively. When radiation force IRFs with and without vertical wall effects are compared, the amplitude of IRFs with vertical wall effects are greater compared to those of without vertical wall effects at longer times although the amplitudes of interaction IRFs are approximately the same at lower times. As in the case of exciting IRFs, the greater amplitude of interaction radiation IRFs at larger times implicitly means that the more wave energy is available to absorb. It may be also noticed that the interaction effects are greater at closer proximity of WECs whilst the greater interaction effects are shifted to longer times when the separation distances between WECs are increased.

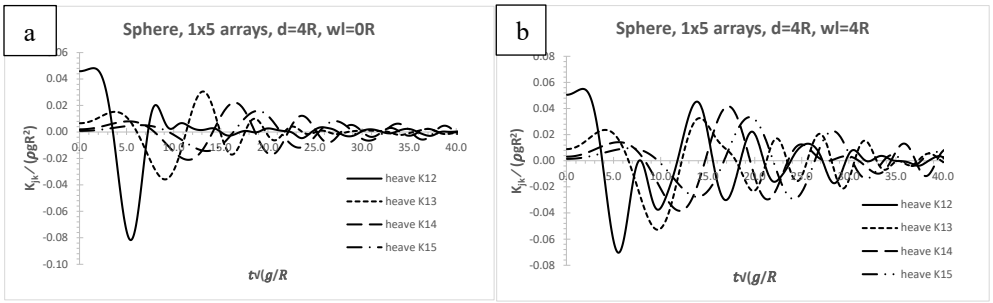

Figure 14. Heave dimensionless radiation interaction IRFs of 1x5 arrays of sphere; (a) without vertical wall effect; (b) with vertical wall effect.

Response Amplitude Operators (RAOs) of WECs in an array system

The sway and heave RAOs with 1x5 arrays of sphere in front of a vertical wall at heading angles 90º are presented in Figure 15(a) and 15(b) respectively. The RAOs for WEC1 and WEC5 as well as WEC2 and WEC4 in Figure 15(b) are the same due to the symmetry of WECs with respect to incident wave angle 90º. It may be also noticed that both sway and heave modes have three resonant frequencies, but magnitude of the resonances are finite.

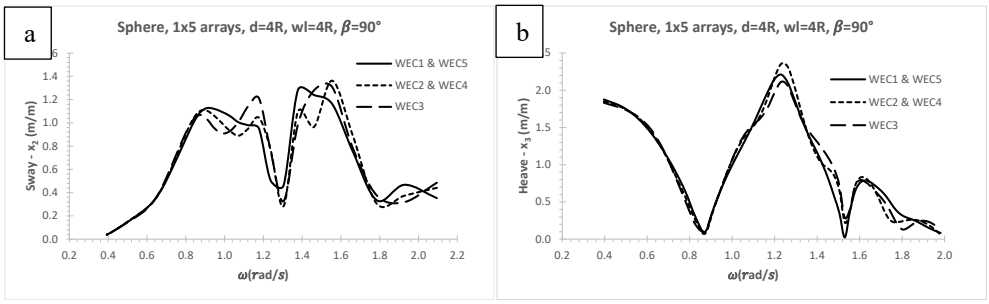

Figure 15. RAOs for each WEC in 1x5 arrays of sphere in front of a vertical wall; (a) sway; (b) heave.

The RAOs for sway and heave modes with 2x5 arrays in front of a vertical wall at heading angle 90º are presented in Figure 16(a), 16(b), 16(c) and 16(d) for 1st and 2nd rows of sway mode as well as 1st and 2nd rows of heave mode respectively. The incident wave meets 1st row WECs first and 2nd row WECs are located at the wake of 1st row. There are five sway resonance and six heave resonance conditions for 1st row WECs. These resonances are finite which means that some of the wave energy at these resonance conditions are radiated back to sea due to oscillations of WECs in an array system. The sway and heave RAOs for 2nd row WECs are greater than those of 1st row due to the standing and nearly trapped waves between gaps of WECs in an array system as well as WECs and a vertical wall. The heave RAOs of WEC1 and WEC5 as well as WEC2 and WEC4 are the same due to symmetry of WECs with respect to incident wave at heading angle 90º.

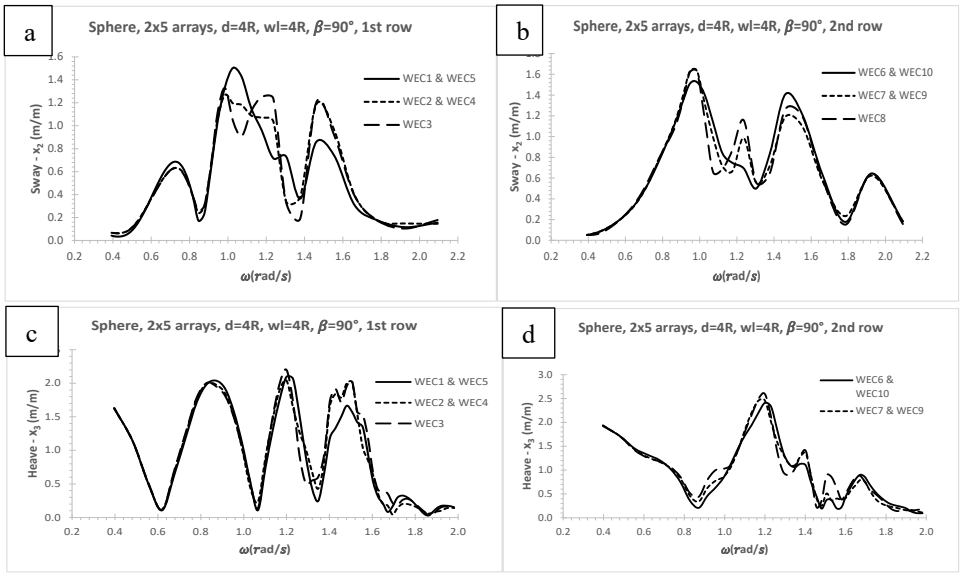

Figure 16. RAOs for each WEC in 2x5 arrays of sphere in front of a vertical wall; (a) sway – 1st row; (b) sway – 2nd row; (c) heave – 1st row; (d) heave – 2nd row.

Absorbed wave power with isolated, 1x5 and 2x5 arrays in front of a vertical wall

The sway and heave RAOs and absorbed wave power with an isolated sphere at heading angle 90º are presented in Figure 17(a) and 17(b) respectively. As floating systems (e.g., sphere WEC) do not have the restoring force at sway mode, it is assumed in the present study that PTO restoring force coefficients at sway and heave modes are equal. This means both sway and heave modes have the same displacements which implies that the performances of sphere at both modes can be directly compared against each other. As it may be observed in Figure 17(b) and is theoretically known (Budal and Falnes 1976) that the maximum wave power is captured at resonant frequency at which natural frequency of sphere (w=1.38 rad/s) at both sway and heave modes are equal to incident wave frequency. It may be noticed in Figure 17(b) that more wave power is absorbed at resonant frequency at sway mode than heave mode. The absorption bandwidth in Figure 17(b) is much wider at sway mode at higher frequencies although heave mode absorbs more power at lower frequencies at which more wave energy is available to absorb.

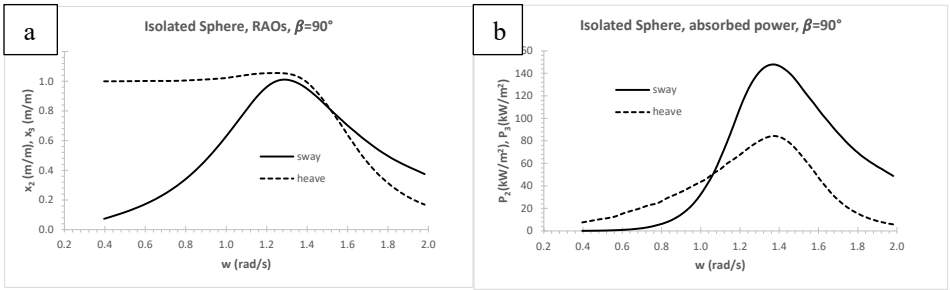

Figure 17. Isolated sphere with radius R in sway and heave modes; (a) RAOs; (b) absorbed power.

The absorbed wave power with 1x5 arrays of sphere in front of a vertical wall at heading angle 90º is presented in Figure 18. It may be noticed that maximum wave power is absorbed at mainly two incident wave frequencies of around 0.83 and 1.56 rad/s in sway mode whilst wave power absorption is concentrated about single incident wave frequency of 1.26 rad/s in heave mode.

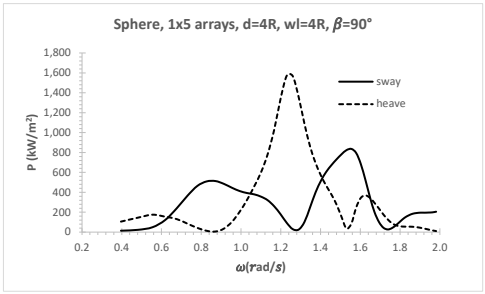

Figure 18. Absorbed wave power in sway and heave modes with 1x5 arrays of sphere in front of a vertical wall.

The absorbed wave power with 1st row, 2nd row and superpositions of 1st and 2nd rows using 2x5 arrays of sphere in front of a vertical wall at heading angles 90º is presented in Figure 19(a) and 19(b) for sway and heave modes respectively. The wave energy absorbtion in heave mode Figure 19(b) is concentrated at wave frequencies of 1.2 and 1.5 rad/s whilst it is distributed in a range of incident wave frequencies with much wider frequency bandwidth in sway mode Figure 19(a). The absorption with sway mode in Figure (19(a) are greater at around incident wave frequency of 1.1 rad/s with 1st row WECs whilst 2nd row WECs, which are at the wake of 1st row, absorb more power at around 0.8 rad/s. The maximum wave power in Figure 19(b) is absorbed at the same incident wave frequency of 1.2 rad/s with 1st and 2nd row WECs with heave mode although 2nd row WECs absorb much greater wave power at incident wave frequency of 1.5 rad/s. The magnitude of absorbed wave power in heave mode is about 2.5 times greater than that of sway mode.

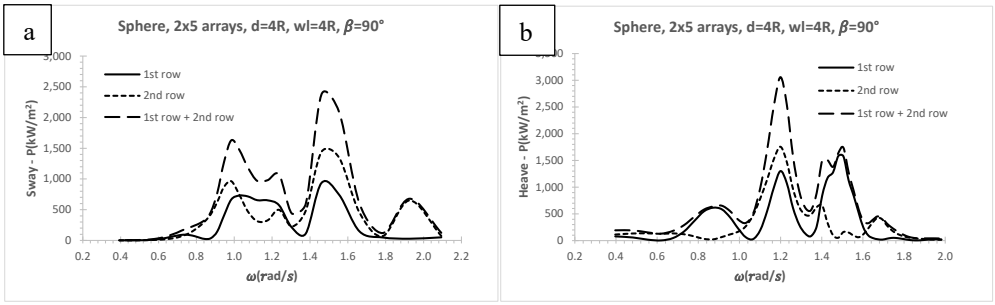

Figure 19. Absorbed wave power with 2x5 arrays of sphere in front of a vertical wall; (a) sway (b) heave mode.

Mean interaction factors with 1x5 and 3x5 arrays of sphere in front of a vertical wall

Mean interaction factors q_{mean} of sway and heave modes are presented for 1x5 and 3x5 arrays of sphere in Figure 20(a) and 20(b) respectively. The sway mode in Figure 20(a) shows high constructive effects up to around incident wave frequency of 1.0 rad/s whilst it shows destructive effects between incident wave frequencies of 1.0 and 1.46 rad/s. When heave mode interaction factor is compared with sway mode in Figure 20(a), the heave mode shows constructive effect in a range of incident wave frequencies apart from around incident wave frequencies of 0.87 and 1.53 rad/s. In the case of 3x5 arrays, the heave mode in Figure 20(b) shows constructive effects almost all range of incident wave frequencies whilst sway mode has very high constructive effect up to the incident wave frequency of 1.0 rad/s.

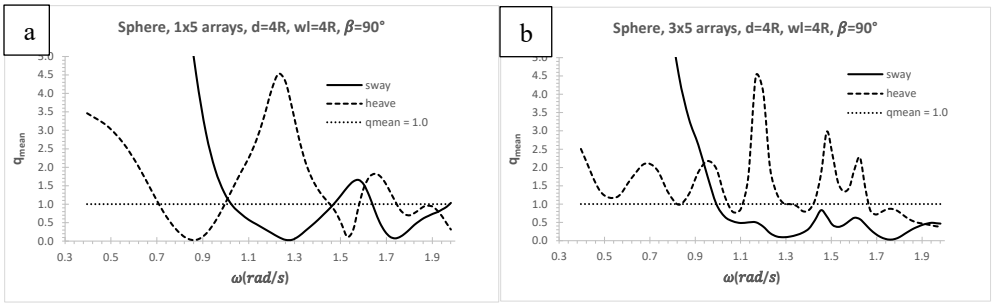

Figure 20. Mean interaction factors of sphere in front of a vertical wall in sway and heave modes; (a) 1x5 arrays; (b) 3x5 arrays.

Mean interaction factors of 3x5 and 5x5 arrays of sphere without a vertical wall effect

Mean interaction factors q_{mean} of each row of sphere with 3x5 and 5x5 arrays are presented in Figure 21(a) and 21(b) respectively. It can be observed that higher row numbers (e.g., 3rd row for 3x5 arrays and 4th and 5th rows for 5x5 arrays) has better constructive effects compared to lower row numbers especially at higher incident wave frequencies (e.g., 1st row) which meet with incident wave first. When the row numbers increase, the destructive effect of lower row numbers increases (e.g., 1st and 2nd rows). This may be noticed when mean interaction factor of 1st rows in Figure 21(a) and 21(b) are compared.

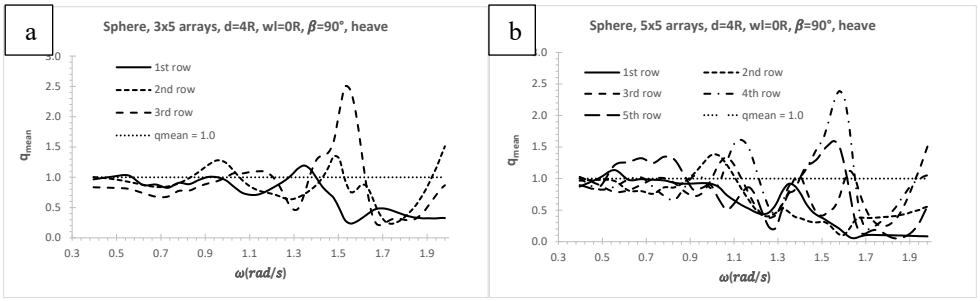

Figure 21. Mean interaction factors of sphere without vertical wall effect in heave mode; (a) 3x5 arrays; (b) 5x5 arrays.

Mean interaction factors of sphere with 3x5 and 5x5 arrays in front of a vertical wall

Mean interaction factors q_{mean} of sphere with 3x5 and 5x5 arrays in front of a vertical wall are presented for each row in Figure 22(a) and 22(b) respectively. It may be noticed that when the rows are closer to vertical wall, mean interaction factors are greater compared to the rows which are away from a vertical wall (e.g., 3rd and 2nd rows for 3x5 sphere arrays whilst 5th and 4th rows for 5x5 arrays). When the row numbers increase in an array system, the contributions of the rows away from a vertical wall to wave absorption in Figure 22(b) are mostly destructive (e.g., 1st, 2nd, and 3rd rows at especially higher frequencies).

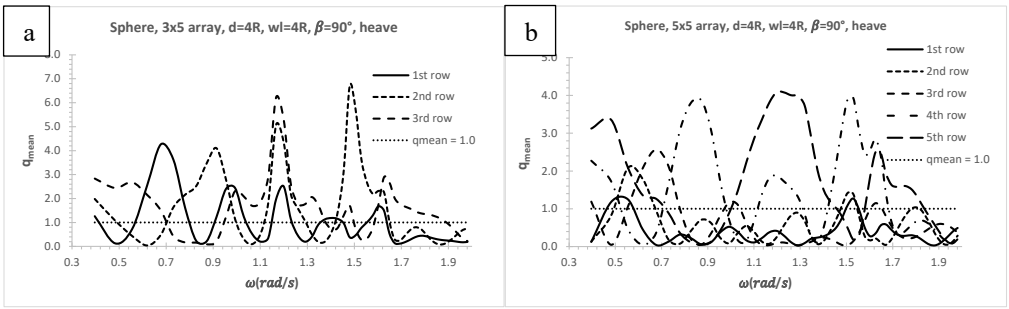

Figure 22. Mean interaction factors of each row of sphere in front of a vertical wall in heave mode; (a) 3x5 arrays; (b) 5x5 arrays.

Mean interaction factors of sphere in a range of arrays with and without a vertical wall effect

Mean interaction factors without and with a vertical wall effect for sphere WECs of 1x5, 2x5, 3x5, 4x5 and 5x5 arrays in heave mode in a range of incident wave frequencies are presented in Figure 23(a) and 23(b) respectively. In the case of 1x5 arrays of sphere in front of a vertical wall, the behaviour of mean interaction factors shows constructive effect apart from about incident wave frequencies of 0.87 and 1.53 rad/s. When other array configurations in front of a vertical wall are considered, mean interaction factors of 2x5,

3x5, 4x5 and 5x5 arrays have the constructive effects in a range of the incident wave frequency up to 1.7 rad/s, however, after this incident wave frequency, mean interaction factors show destructive effects. The magnitudes of the constructive effects decrease with increasing row numbers at lower incident wave frequencies in Figure 23(b). Mean interaction factors of 2x5, 3x5, and 4x5 arrays in Figure 23(b) also show 2.2 times constructive effects up to incident wave frequency of 1.1 rad/s whilst the constructive effects of 1x5, 2x5, and 3x5 arrays reach up to 4.65 times at incident wave frequency of 1.2 rad/s. However, these constructive effects decrease up to 2.3 and 1.4 for 4x5 and 5x5 arrays at the same incident wave frequency of 1.2 rad/s respectively. In the case of arrays without a vertical wall effect, the dominant incident wave frequency is around 1.5 rad/s for constructive effect whilst it is around 1.75 rad/s for destructive effect. When with and without a vertical wall effect are compared, it can be clearly observed from Figure 23(a) and (b) that the magnitudes of the constructive effects of WECs arrays in front of a vertical wall in Figure 23(b) are much greater almost all range of incident wave frequencies compared to without a vertical wall effect in Figure 23(a).

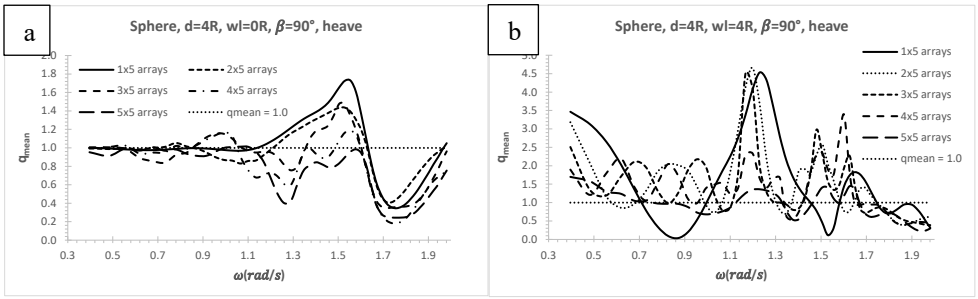

Figure 23. Mean interaction factors of sphere in heave mode in a range of row numbers and 5 column numbers; (a) without a vertical wall effect; (b) with a vertical wall effect.

Wave energy converters with latching control

Latching control, which is a discrete real time control, is used in the present paper. Rather than adapting WEC parameters to the excitation force to optimize the linear body response, the latching control adapts the body response to WEC and to the excitation in a nonlinear fashion. It is a kind of parametric resonance adaptation process as can be found in nonlinear oscillatory theory; this kind of behaviour can be predicted only using time domain simulations. Latching control can magnify the amplitude of the motion whatever the frequency of the excitation force and can improve the efficiency of WEC.

When latching control is applied, an additional force must be introduced in the dynamic of WEC to cancel the acceleration of the controlled motion to lock the system temporarily. The latching control of WEC consists of locking the oscillating body in position at the instant when velocity vanishes and releasing it after a certain delay to be determined. This latching delay must be applied to maximise the response amplitude of the body. The instant

of latching is imposed by the dynamics of the body itself (i.e., vanishing velocity); thus, the control variable is simply the duration of the latching phase, or equivalently the instant of release (Greenhow et.al. 1997, Eidsmoen 1998, Kara 2010, 2021b). One of the advantages of latching control is that it is passive, which means that it does not need to deliver energy to WEC while it is engaged, since the forces do no work if the velocity vanishes.

Instantaneous and mean absorbed power

Figure 24 (a) shows the instantaneous power absorbed for incident wave period of 15s from ocean waves using a vertical cylinder with sphere bottom (which has 8m radius, 13m draft and free to heave mode and fixed for other modes) as a wave energy converter with and without latching control. In the case of latching control, the absorbed instantaneous power is increased significantly. It may be noticed that the unlatching results are very small in terms of controlled latching results. Figure 24 (b) shows also the absorbed mean power for the range of incident wave frequencies. In the case of latching control, the absorbed mean power is increased significantly. The theoretical maximum power $P = \rho g^3 \zeta_a/(4\omega^3)$ in regular seas (Budal and Falnes, 1976) is compared with ITU-WAVE numerical results. As can be seen from Figure 24 (a) the absorbed mean power at low frequencies which has more power compared to high frequencies are increased significantly with latching control.

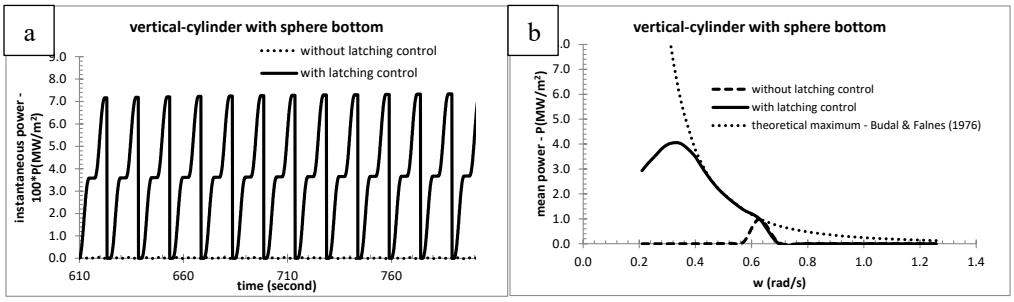

Figure 24. Instantaneous power (a) absorbed by a vertical cylinder with sphere bottom at each period with and without latching control at resonance period at 10s and incident wave period at 15s with 1m wave amplitude, absorbed mean power (b) with and without latching control in the range of frequencies.

Efficiency

The efficiency η of WECs is defined as $\eta = l/l_{max}$ which has a maximum of 1.0 for any wavelength. The capture width l and maximum capture width l_{max} is defined as (Budal and Falnes, 1976) $l = \bar{P}_{ins_k}/P_w$ and $l_{max} = \lambda/(2\pi)$ where $\bar{P}_{ins_k}(t)$ is the mean power and given by Eq. (11), $P_w = \rho g^2 \zeta_a^2/(4\omega)$ is the wave power in the incident wave train per

unit crest length, ζ_a being the incident wave amplitude. A good wave absorber is a body which has the ability when making waves, to concentrate the wave energy along a narrow sector rather than distribute the energy evenly over all angles. The maximum capture width equals to $l_{max} = \lambda/(2\pi)$ for an axisymmetric system in symmetric mode of motion e.g., heave. This implies that the floating body absorbs all the power in an incident wave equal to that passing a crest length of $\lambda/(2\pi)$.

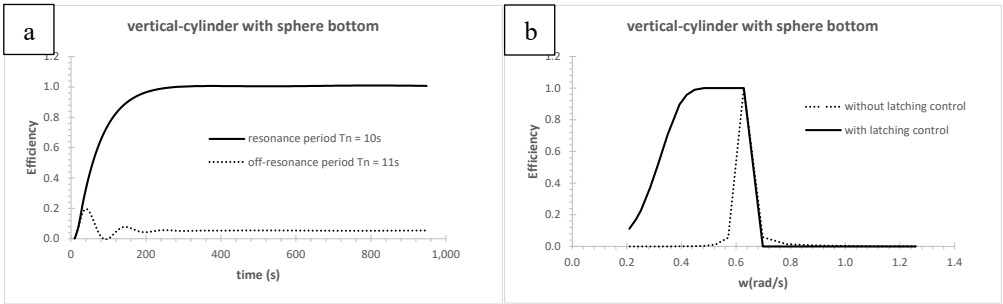

Figure 25. Convergence of efficiency for resonance and off-resonance period without latching control for a vertical-cylinder with sphere bottom (a) and efficiency with and without latching control at a range of frequencies (b).

Figure 25 (a) shows the efficiencies for vertical-cylinder with sphere bottom in the case of in resonance and off-resonance periods. The efficiency converges to 1.0 (100% efficient) at resonance period $T_n = 10s$ whereas off-resonance case $T = 11s$ shows a very low efficiency (5%). Figure 25 (b) shows the efficiency plotted at a range of frequencies. If the natural period of vertical cylinder equals the period of incident waves in the case of without latching control, the device is perfectly tuned, and we expect optimal efficiency. As the difference between natural period of device and incident wave period increases, the efficiency of the system decreases. As can be seen in Figure 25 (b) latching control increases the bandwidth of the wave energy converter for lower frequency ranges. If off-resonance period is 11s (0.571 rad/s), the efficiency is approximately 5% without latching control. However, if $1s$ latching is applied, it is possible to achieve an efficiency of approximately 100%.

CONCLUSION

The exploitation of the wave power absorption from ocean waves using WECs arrays with and without a vertical wall effect is analysed with in-house transient wave-multibody interaction computational tool of ITU-WAVE. The time dependent boundary integral equation method is used to solve the initial boundary value problem with time marching scheme whilst the perfect reflection of the incident waves from a vertical wall is predicted with method of images in ITU-WAVE numerical tool.

The amplitudes of the diagonal and interaction radiation IRFs are comparable at closer proximity. This implicitly means that WECs in an array system have strong hydrodynamic interactions due to standing waves and nearly trapped waves in the gap of WECs and a vertical wall. The numerical experiences also show that when the separation distances between WECs as well as WECs and a vertical wall increase, the interaction effects are getting weaker which means available wave energy to absorb from ocean waves decreases. In the case of wave exciting forces, exciting force IRFs with and without vertical wall effects are compared, it is observed that the bandwidth of exciting force IRFs with a vertical wall effect are greater which means that the available energy to absorb are also greater.

The nearly trapped and standing waves in the gap of WECs as well as WECs and a vertical wall in an array system play significant role for the maximum wave power absorption especially closer separation distances. It is found out by the numerical experiences that the mean interaction factors for all considered array systems are at least 2 times greater in the case of arrays in front of a vertical wall compared to arrays without a vertical wall effect. The constructive effect is also much greater than destructive effect in an array system in front of a vertical wall for all considered array systems.

The numerical results show that the efficiency of WEC is considerably improved by the latching control which enlarges the bandwidth of WEC in the low frequencies, if the exciting force is predicted in the close future of the unlatching time and that body is hold in position during the latching time. The numerical experience also showed that the decision to release or not WEC at a current time depends on the future of the system beyond the current time. The better this quantity can be predicted, the closer the converted power may approach the theoretical maximum.

REFERENCES

Budal, K. (1977). Theory for absorption of wave power by a system of interacting bodies. Journal of Ship Research, 21(4), 248-253.

Budal, K., Falnes, J. (1976). Optimum operation of wave power converter. Internal Report, Norwegian University of Science and Technology.

Chang, M.S. (1997). Computation of Three-Dimensional Ship Motions with Forward Speed. Proceedings of the 2nd International Symposium on Numerical Ship Hydrodynamics, University of California, Berkeley, 124-135.

Chatjigeorgiou, I.K. (2019). Semi-analytical solution for the water wave diffraction by arrays of truncated circular cylinders in front of a vertical wall. Applied Ocean Research, 88, 147-159.

Contestabile, P., Di Lauro, E., Buccino, M. and Vicinanza, D. (2016). Economic assessment of overtopping breakwater for energy conversion (OBREC): a case study in western Australia. Sustainability, 9(1), 51.

Cummins, W.E. (1962). The Impulse response function and ship motions. Shiffstechnik, 9, 101-109.

Eidsmoen, H. (1998). Tight-moored amplitude limited heaving buoy wave energy converter with phase control. Applied Ocean Research, 20, 157-161.

Greenhow, M. and White, S.P. (1987). Optimal heave motion of some axisymmetric wave energy devices in sinusoidal waves. Applied Ocean Research, 19, 141-159

He, F., Huang, Z.H. and Law, A.W.K. (2013). An experimental study of a floating breakwater with asymmetric pneumatic chambers for wave energy extraction. Applied Energy, 106, 222-231.

Hess, J.L. and Smith, A.M.O. (1964). Calculation of non-lifting potential flow about arbitrary three-dimensional bodies. Journal of Ship Research, 8, 22-44.

Kagemoto, H. and Yue, D.K.P. (1986). Interactions among multiple three-dimensional bodies in water waves: an exact algebraic method. Journal of Fluid Mechanics, 166, 189-209.

Kara F, 2021a. Hydrodynamic performances of wave energy converters arrays in front of a vertical wall. *Ocean Engineering, 235, 109459.*

Kara F, 2021b. Applications of time domain methods for marine hydrodynamic and hydroelasticity analyses of floating systems. *Ships and Offshore Structures,* https://doi.org/10.1080/17445302.2021.1937798

Kara F, 2021c. Hydroelastic behaviour and analysis of marine structures. *Journal of Sustainable Marine Structures, 2(1), 14-24.*

Kara F, 2020a. A Control strategy to improve the efficiency of point absorber wave energy converters in complex sea environments. *Journal of Marine Science Research and Oceanography, 3(2), 43-52.*

Kara, F. (2020b). Multibody interactions of floating bodies with time domain predictions. Journal of Waterway, Port, Coastal, and Ocean Engineering, 146(5).

Kara F, 2017. Control of wave energy converters for maximum power absorptions with time domain analysis. *Journal of Fundamentals of Renewable Energy and Applications, 7(1), 1-8*

Kara, F. (2016a). Time domain prediction of power absorption from ocean waves with wave energy converters arrays. Renewable Energy, 92, 30-46.

Kara, F. (2016b). Time domain prediction of seakeeping behaviour of catamarans. International Shipbuilding Progress, 62(3-4).

Kara F, 2016c. Point absorber wave energy converter in regular and irregular waves with time domain analysis. *International Journal of Marine Science and Ocean Technology, 3(7), 74-85.*

Kara, F. (2015). Time domain prediction of hydroelasticity of floating bodies. Applied Ocean Research, 51, 1-13.

Kara F, 2011. Time Domain Prediction of Added Resistance of Ships. *Journal of Ship Research, 55 (3), 163-184*

Kara, F. (2010). Time domain prediction of power absorption from ocean waves with latching control. Renewable Energy, 35, 423-434.

Kara, F. (2000). Time domain hydrodynamics and hydroelastics analysis of floating bodies with forward speed. PhD thesis, University of Strathclyde, Glasgow, UK.

King, B.W. (1987). Time Domain Analysis of Wave Exciting Forces on Ships and Bodies. PhD thesis, The University of Michigan, Ann Arbor, Michigan, USA.

Konispoliatis, D.N., Mavrakos, S.A. and Katsaounis, G.M. (2020). Theoretical evaluation of the hydrodynamic characteristics of arrays of vertical axisymmetric floaters of arbitrary shape in front of a vertical breakwater. Journal of Marine Science and Engineering, 8, 62.

Kring, D.C. and Sclavounos, P.D. (1995). Numerical stability analysis for time-domain ship motion simulations Journal of Ship Research, 39 (4), 313-320.

Liapis, S. (1986). Time Domain Analysis of Ship Motions. PhD thesis, The University of Michigan, Ann Arbor, Michigan, USA.

Loukogeorgaki, E., Boufidi, I. and Chatjigeorgiou, I.K. (2020). Performance of an array of oblate spheroidal heaving wave energy converters in front of a wall. Water, 12, 188.

McCallum, P., Venugopal, V., Forehand, D. and Sykes, R. (2014). On the performance of an array of floating wave energy converters for different water depths. Proceedings of the ASME, 33rd International Conference on Ocean, Offshore and Arctic Engineering, OMEA2014, June 8-13, USA.

McIver, P. and Porter, R. (2016). The motion of a freely floating cylinder in the presence of a wall and the approximation of resonances. Journal of Fluid Mechanics, 795, 581–610.

Mustapa, M.A., Yaakob, O.B., Ahmed, Y.M., Rheem, C.-K, Koh, K.K. and Adnan, F.A. (2017). Wave energy device and breakwater integration: A review. Renewable and Sustainable Energy Reviews, 77, 43–58.

Nakos, D., Kring, D. And Sclavounos, P.D. (1993). Rankine Panel Method for Transient Free Surface Flows. Proceedings of the 6th International Symposium on Numerical Hydrodynamics, Iowa City, I.A., USA, 613-632.

Newman, J.N. (2016). Channel wall effects in radiation-diffraction analysis, 31st International Workshop on Water Waves and Floating Bodies.

Ning, D.Z., Zhao, X.L., Goteman, M. and Kang, H.G. (2016). Hydrodynamic performance of a pile-restrained WEC-type floating breakwater: an experimental study. Renew Energy, 95, 531-541.

Ogilvie, T.F. (1964). Recent progress toward the understanding and prediction of ship motions. Proceedings of the 5th Symposium on Naval Hydrodynamics, Office of Naval Research, Washington, D.C., USA, 3-128.

Ohkusu, M. (1972). Wave action on groups of vertical circular cylinders. Journal of the Society of Naval Architects in Japan, 131.

Schay, J., Bhattacharjee, J. and Soares, C.G. (2013). Numerical Modelling of a Heaving Point Absorber in front of a Vertical Wall. In Proceedings of the ASME 32nd International Conference on Ocean, Offshore and Arctic Engineering, Nantes, France, 9–14 June.

Thomas, G.P. and Evans, D.V. (1981). Arrays of three-dimensional wave-energy absorbers. Journal of Fluid Mechanics, 108, 67-88.

Wehausen, J.V. and Laitone, E.V. (1960). Surface Waves in Fluid Dynamics III in Handbuch der Physik; Chapter 3:446-778

Zhao, X.L., Ning, D.Z., Zou, Q.P., Qiao, D.S. and Cai, S.Q. (2019a). Hybrid floating breakwater-WEC system: A review. Ocean Engineering, 186, 106-126.

Zhao, X.L., Ning, D.Z. and Liang, D.F. (2019b). Experimental investigation on hydrodynamic performance of a breakwater integrated WEC system. Ocean Engineering, 171, 25-32.

Zheng, S. and Zhang, Y. (2016). Wave radiation from a truncated cylinder in front of a vertical wall. Ocean Engineering, 111, 602–614.